Short communication

Nature of LiFePO$_4$ aging process: Roles of impurity phases

Jiajun Wang [a], Yongji Tang [a], Jinli Yang [a], Ruying Li [a], Guoxian Liang [b], Xueliang Sun [a],*

[a] Department of Mechanical and Materials Engineering, University of Western Ontario, London, ON, Canada N6A 5B9
[b] Phostech Lithium Inc., 1475, rue Marie-Victorin, St-Bruno, QC, Canada J3V 6B7

HIGHLIGHTS

- Surface corrosion process at olivine LiFePO$_4$ was directly observed.
- The direct relationship between impurity phases and LiFePO$_4$ corrosion was presented.
- A deep understanding the underlying mechanism in the LiFePO$_4$ aging was provided.

GRAPHICAL ABSTRACT
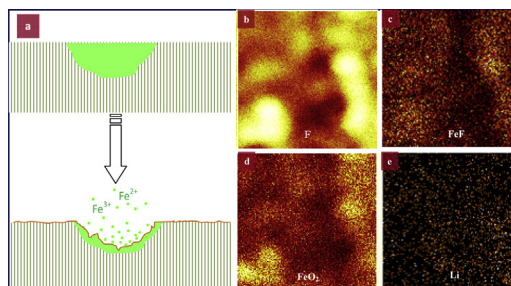
ABSTRACT

LiFePO$_4$ has been extensively studied in recent years because of superior thermal stability for the next generation of lithium-ion batteries. Nevertheless, LiFePO$_4$ still undergo iron dissolution at high temperature or moisture-contaminated electrolyte, and the detailed mechanism is still not clear. Few efforts have been devoted to the correlations between surface chemistry and aging mechanisms. Here, we present a direct visual observation of surface corrosion process at olivine LiFePO$_4$, and found the direct relationship between impurity phases and LiFePO$_4$ corrosion. By using the LiFePO$_4$ ingot sample with a flat surface as model materials, two types of impurity phase (iron-rich and phosphorus-rich) can be clearly observed and their influences on LiFePO$_4$ corrosion were investigated in detail by SEM, Tof-SIMS, and electrochemical Tafel analysis. Similar to the electrochemical cell mechanism in a common metal corrosion process, an oxidation–reduction mechanism was suggested at the impurity phases-relevant corrosion behavior. Iron-rich impurity phases are seriously corroded due to the lower corrosion potentials, which inhibit the corrosion of the adjacent LiFePO$_4$ bulk. On the contrary, phosphorus-rich impurity phase is stable due to higher corrosion potentials, which evokes the serious corrosion occurring at the adjacent LiFePO$_4$ bulk. These findings provide the deep understanding the underlying mechanism in the LiFePO$_4$ aging.

© 2013 Elsevier B.V. All rights reserved.

1. Introduction

LiFePO$_4$ olivine has been extensively studied and developed in recent years for the next generation of lithium-ion batteries because of its high structure stability and superior cycle performance since its discovery in 1997 [1–3]. Compared with some conventional oxides cathodes such as LiCoO$_2$ which suffers the structural change or detrimental interaction with electrolyte at high charging potentials, LiFePO$_4$ can undergo full lithiation–delithiation process without obvious structural change due to a strong covalent P–O bonds in (PO$_4$)$^{3-}$ polyanion, which makes them the excellent stable and safe cathode materials [4,5].

Nevertheless, it was reported that LiFePO$_4$ still suffered fast capacity fading at high temperature and/or moisture-contaminated

---

* Corresponding author.
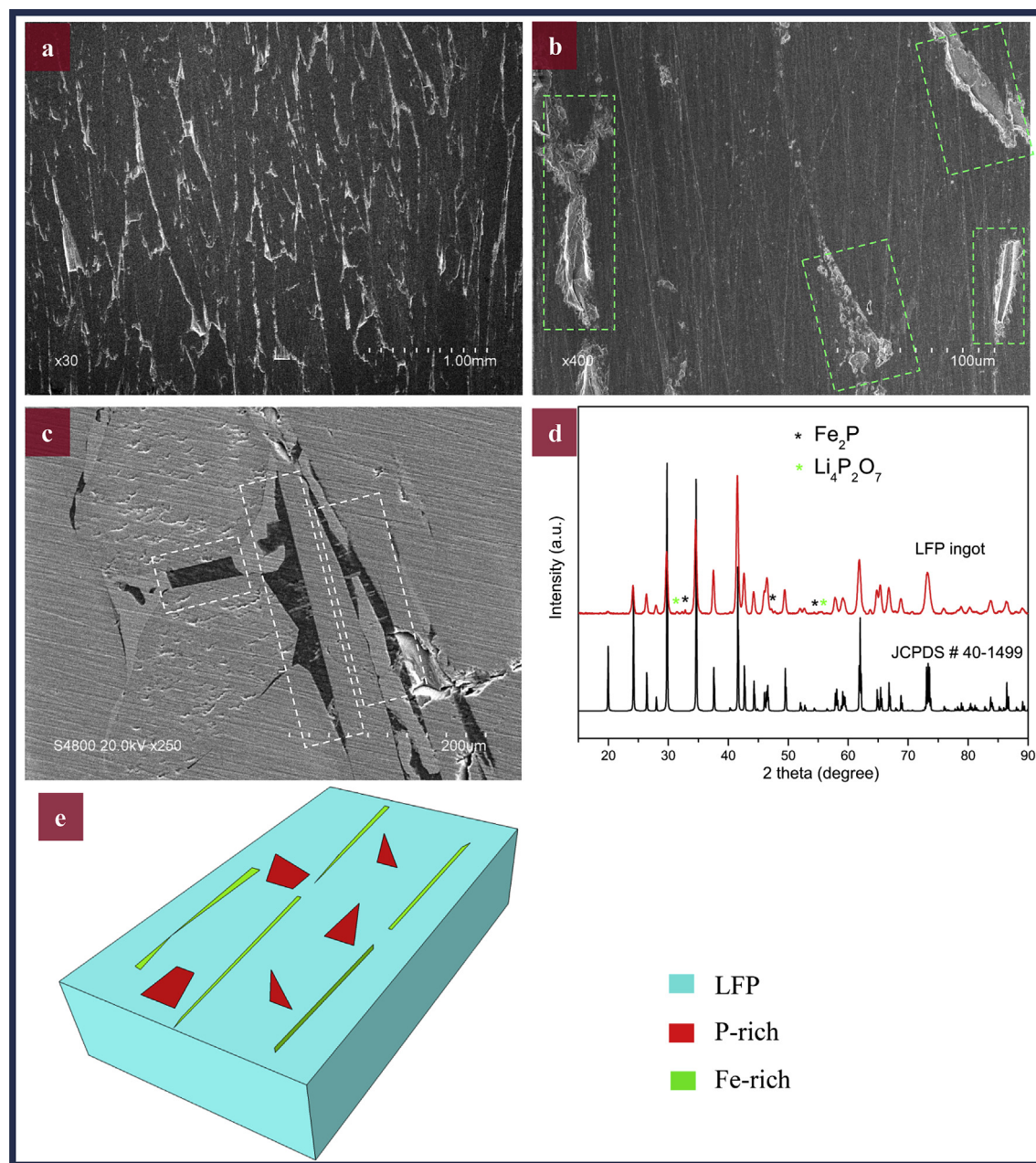E-mail address: xsun@eng.uwo.ca (X. Sun).

Fig. 1. SEM images of the ingot LiFePO$_4$ surface (a), iron-rich impurities (b), and phosphorus-rich impurities (c), (d) XRD patterns of the ingot sample, (e) a schematic illustration of ingot LiFePO$_4$ with impurity phases.

electrolyte [6–10]. For example, Amine et al. revealed that no significant capacity loss for LiFePO$_4$ was found after 100 cycles at room temperature, but over 60% capacity fading occurred when it was operated at 55 °C [10]. The accelerated capacity loss was attributed to iron dissolution from LiFePO$_4$ attacked by acid species such as HF in moisture-contaminated LiPF$_6$ electrolyte [11–13]. Moreover high operating temperature will further accelerate the HF formation and the iron dissolution process. Along with the iron dissolution, the irreversible structural change occurs at the active material, and some inactive phases could be formed on the active material, affecting the kinetic process of lithium lithiation–delithiation. Further, the transition metal can move to the negative and be reduced to metallic clusters, resulting in the formation of solid electrolyte interphase, further capacity loss and serious safety issues [14,15].

Considering iron dissolution and related material stability, aging study of LiFePO$_4$ has attracted more and more attentions. There are more and more studies working on the evaluation of LiFePO$_4$ cell performance fading subject to operating conditions such as various electrolytes, temperatures and cell structure as well as detailed degradation mechanism [16–20]. While these outstanding work are necessary and critical for understanding the aging behavior of LiFePO$_4$ based cell, however, few studies worked on the surface chemistry of LiFePO$_4$ material itself and especially the relationship between surface aging process and inhomogeneous surface chemistry (impurity phases). It is well known that some common impurity phases (e.g. Fe$_2$O$_3$, Fe$_2$P, Li$_3$PO$_4$, etc.) often exist accompanying with LiFePO$_4$ synthesis and production [21–24]. As inactive materials, the presence of these impurity phases decreases utilization of LiFePO$_4$, and it also affects significantly the physical
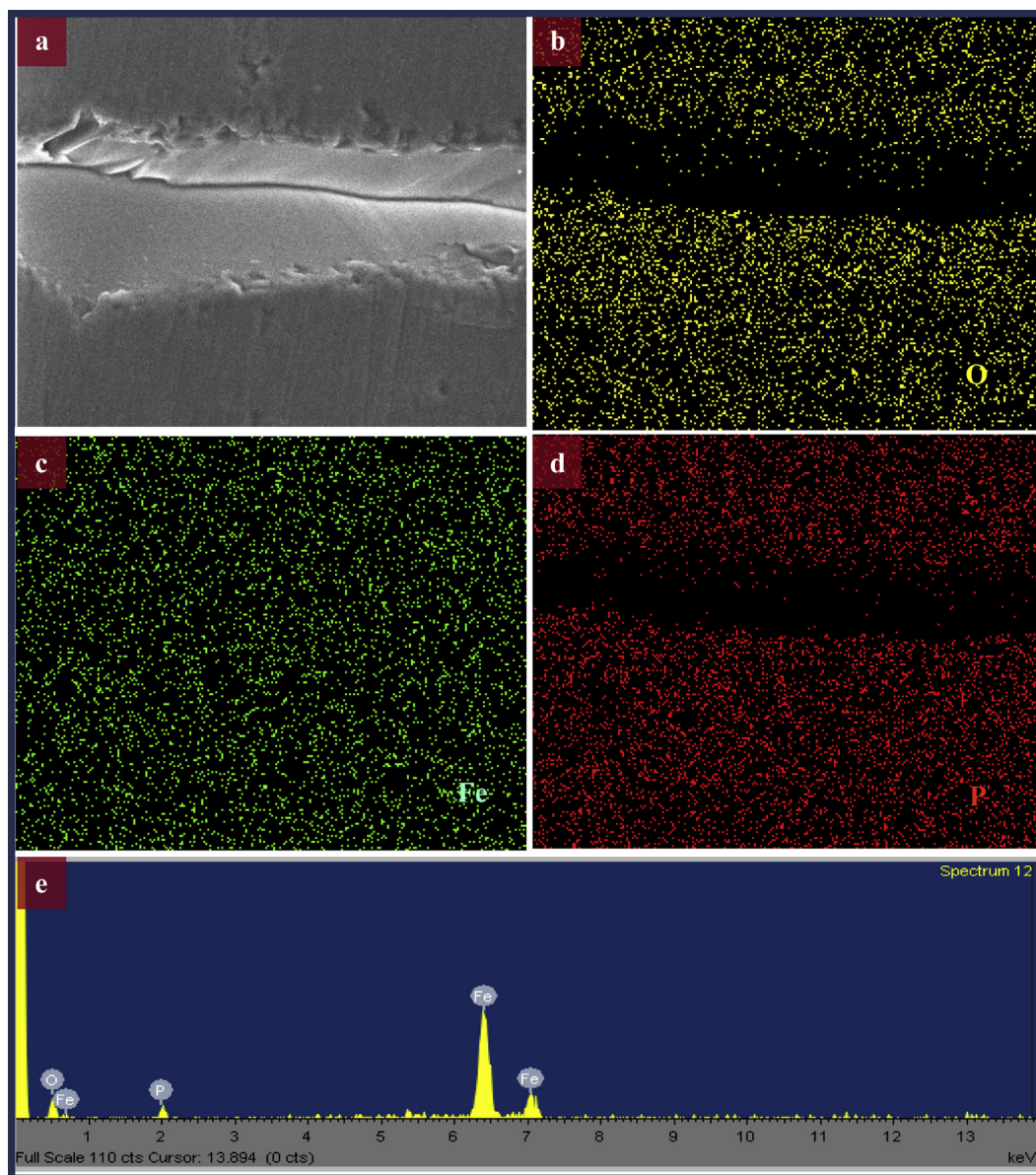
Fig. 2. SEM element mapping of iron-rich impurity phases.

and electrochemical property of LiFePO$_4$ such as the material stability. Therefore, the study of impurity phases and their influence on the stability of LiFePO$_4$ is critical for application of this promising material.

One critical challenge to understand these questions is lack of suitable model LiFePO$_4$ material and tools to directly observe the surface change. We recently overcome this challenge by using molten technique to achieve an ingot sample with a big flat surface. While the ingot sample produced by molten technique can be further ball-milling to various grades of LiFePO$_4$ particles for practical applications in Li ion batteries [25—27], the big flat surface of the ingot sample allows us to directly study the surface aging process. This paper is to present a direct evidence of the relationship between impurity phases and LiFePO$_4$ corrosion under moisture-contaminated electrolyte which is an accelerated corrosive medium to simulate the practical application conditions. By applying various materials characterization tools and working on a model LiFePO$_4$ material, the impurity phases were directly observed and

identified. The aging experiments indicated that the presence of impurity phases or the inhomogeneity of surface chemistry has significant influence on LiFePO$_4$ corrosion. The further electrochemical techniques such as Tafel analysis helped us to understand the correlations between impurity phase and LiFePO$_4$ bulk material. The possible aging mechanism with the presence of impurity phases was also proposed.

2. Experimental section

2.1. Materials and aging experiments

LiFePO$_4$ ingot sample was provided by Phostech Lithium Inc. The ingot sample was prepared by a melt casting process recently developed by Phostech [25]. Here, to get a flat surface on the ingot sample, the melt sample was cut into small size (cm) by a manual saw, and then the surface was polished by various Aluminum Oxide sand papers from coarse (Grit 120) to fine grades (Grit 1500). After
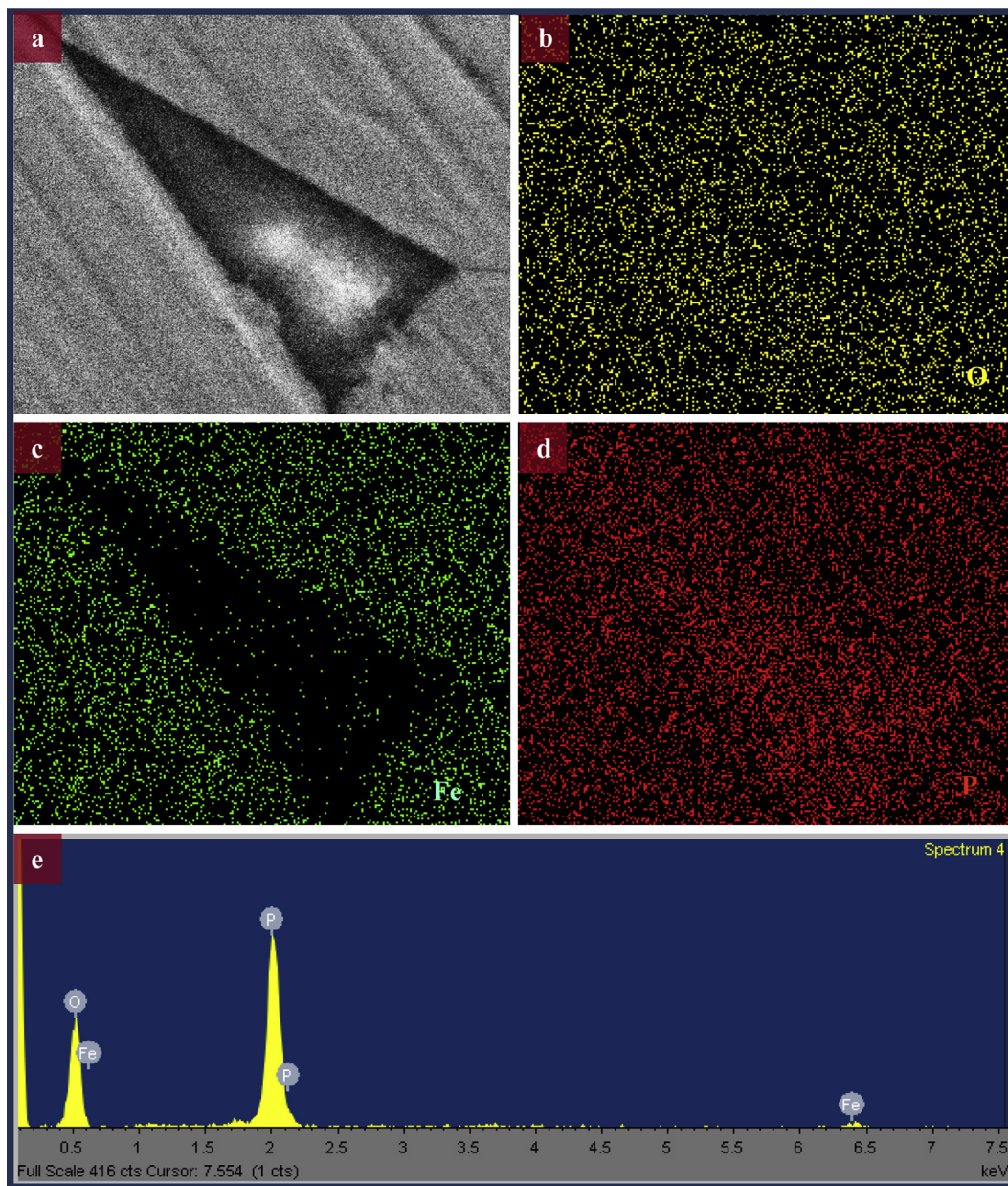
Fig. 3. SEM element mapping of phosphorus-rich phases.

ultrasonic cleaning in ethanol several times, LiFePO$_4$ ingot sample with a clean and flat surface was thus obtained.

The aging experiment was carried out in a moisture-contaminated electrolyte at room temperature. In order to accelerate the aging process, 400 ppm of water was added into the commercial 1 M LiPF$_6$ in EC–DMC 1:1 mixture to promote the HF formation. The polished LiFePO$_4$ ingot sample was stored in this water-contaminated electrolyte for corrosion observation.

2.2. Physical characterizations

The morphology and microstructure of the samples were characterized with an S-4800 scanning electron microscope (SEM, Hitachi) equipped with an energy-dispersive X-ray microanalysis system and a field-emission gun. To confirm the surface chemistry change after aging process, the aged LiFePO$_4$ materials were examined using a time-of-flight-secondary ion mass spectroscopy

(ToF-SIMS, ION-TOF-SIMS IV) surface analyzer. The surface was cleaned by sputtering 10 keV C$_{60}$+ for 2 min. A 25 keV Bi^{3+} primary was used to generate the secondary ions to be analyzed by ToF-SIMS.

2.3. Electrochemical measurements

The electrochemical measurements were performed in a traditional three-electrode system in the moisture-contaminated (400 ppm H$_2$O) commercial 1 M LiPF$_6$ in EC–DMC 1:1 mixture solution utilizing Pt wire as the reference electrode, another Pt wire as the counter electrode, and the sample of several typical commercial impurity phases as the working electrode. A glassy carbon disk electrode was used as a substrate for the working electrode. Prior to test, the electrode was polished with alumina (diameter 0.05 μm) to obtain a mirror finish. A typical suspension of the sample ink was prepared by dispersing an amount of the impurity
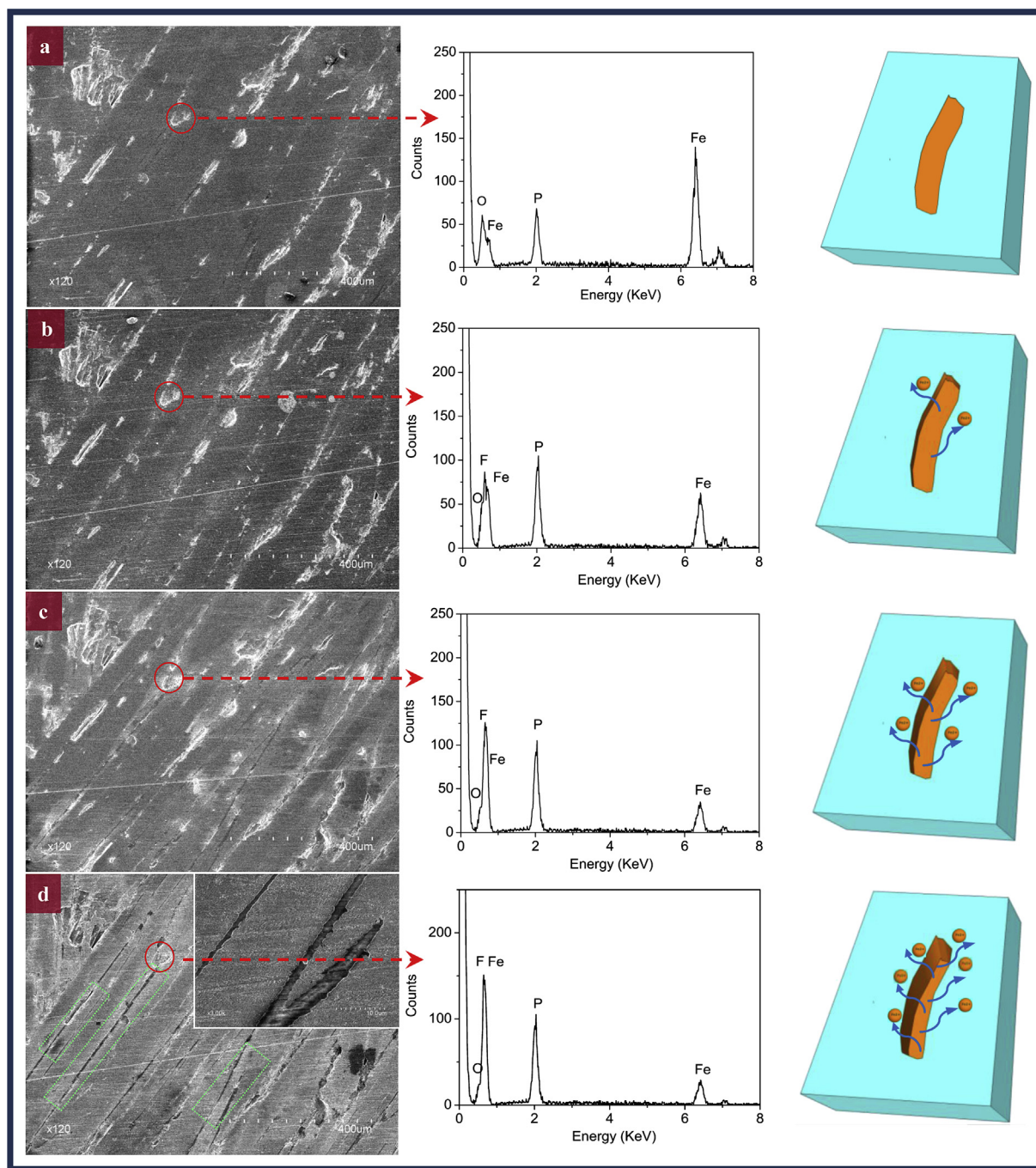
Fig. 4. SEM and EDX with LiFePO$_4$ ingot grain boundaries (iron-rich phases) during surface aging process at 0 h (a), 8 h (b), 24 (c) and 32 h (d).

powder in an isopropanol + Nafion solution. Then 10 μL of this ink was pipetted onto the surface of the electrode and dried in air at room temperature. Prior to the electrochemical test, the electrode was immersed in commercial LiPF$_6$ electrolyte to allow the formation of Li-ion-exchanged Nafion dispersion. The variation of open circuit potential with time was measured since the first minutes of electrodes immersion in the electrolyte solution. The polarization curves were obtained at a scan rate of 0.2 mV s^{-1}. All these electrochemical measurements were performed at an Autolab Potentiostat/Galvanostat (PGSTAT-30, Brinkmann Instruments) at 25 °C.

3. Results and discussion

A model LiFePO$_4$ material (Phostech LiFePO$_4$ ingot) with flat surface polished by sand papers was investigated in this work. This polished surface of LiFePO$_4$ makes it feasible to directly observe its surface aging process. Here some impurity phases can be also directly seen and their effects on surface aging of LiFePO$_4$ were investigated. Fig. 1 shows the SEM image of a fresh polished ingot sample. It is clearly seen that some grain boundaries are distributed on the surface, which is associated with one type of the impurity phase. As shown in Fig. 1b, the first impurity phase with bright
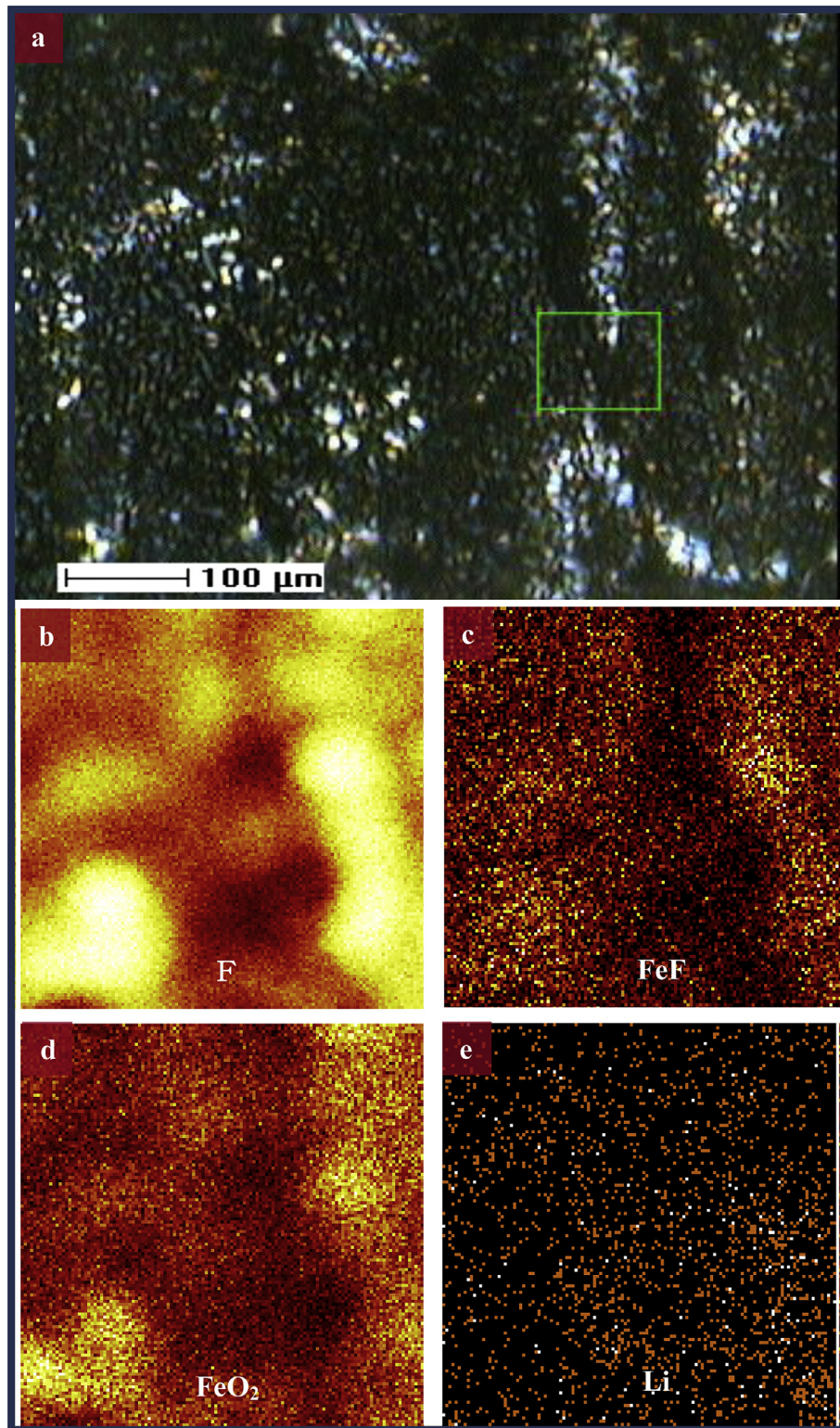
Fig. 5. TOF-SIMS maps of grain boundaries (iron-rich zones) at the aged LiFePO$_4$.

color and irregular shape (marked with dashed rectangle) was mainly located at local defects or porosities around the grain boundaries on the ingot sample where lithium could be lost and the crystal surface is reduced to iron phosphides. The other impurity phases (Fig. 1c) with dark color and flat surface were found to be distributed at the regions near to grain boundaries, as marked with

dashed rectangle. In order to identify these impurity phases, micro-X-ray diffraction pattern was collected and shown in Fig. 1d. The pattern indicates that the ingot is mainly LiFePO$_4$ containing a small amount of impurity phases such as Li$_4$P$_2$O$_7$ (P-rich phases) and Fe$_2$P (Fe-rich phases), and other possible negligible phases. A schematic illustration of LiFePO$_4$ ingot with impurity phases was shown in
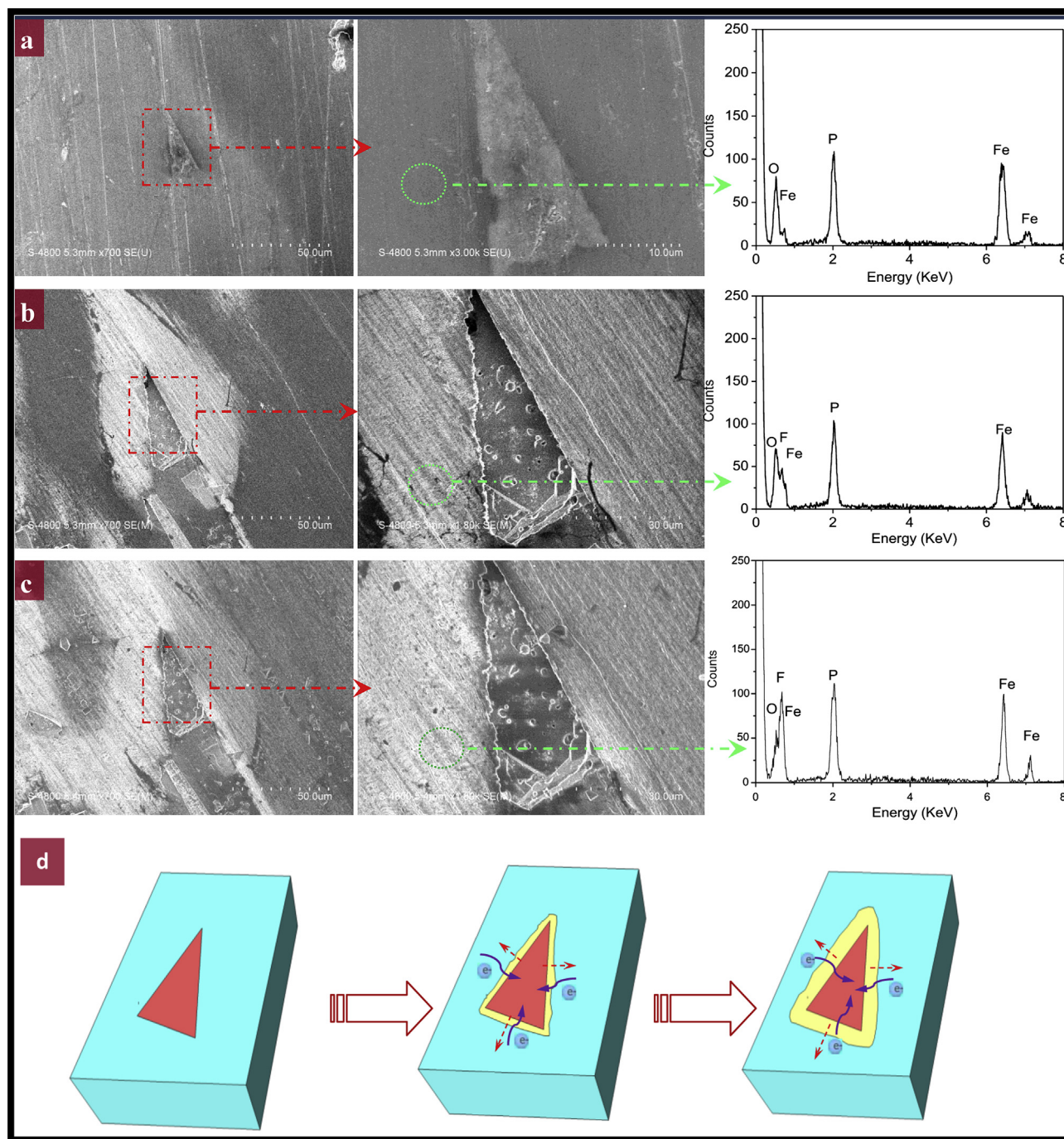
Fig. 6. SEM of P-rich zones and EDX of the adjacent LiFePO$_4$ bulk zone during aging process at 0 h (a), 8 h (b), 32 h (c), and a schematic illustration of corrosion process (d).

Fig. 1e. These typical impurity phases are also detected by other studies using various synthesis methods [28–30].

These impurity phases can be further identified by element mapping and EDX. Fig. 2 shows the element maps and the EDX analysis of the first type of impurity phase. From the element mapping, it can be clearly seen that both oxygen and phosphorus are deficient at the phase. Instead, iron is rich at these phases. The EDX result indicates that the relative atomic ratio for Fe, P, and O is 56:15:29. Therefore, we call this impurity as iron-rich impurity phase (mainly Fe$_2$P). Fig. 3 shows information of the other impurity phases (mainly Li$_4$P$_2$O$_7$). The element mapping shows that this dark zone is an impurity phase with iron-deficient and phosphorus-rich (low Fe/P

ratio) while oxygen element was found to be homogeneously distributed on the entire surface. EDX analysis further indicates that the dark zone shows 5:30:65 for the relative atomic ratio of Fe, P, and O. Detailed characterization of these impurity phases in this ingot sample has been reported in our previous work [31].

All the above observations confirm that the existence of these two types of the impurity phase on the surface of ingot sample. The formation of these impurity phases is related to the metallurgical processes of molten technique [25,26]. During the cooling process, a fractional crystallization from melt of the remaining liquid phase present when LiFePO$_4$ crystallizes, and the excess nonstoichiometric reactants are rejected from LiFePO$_4$ crystals, thus making these
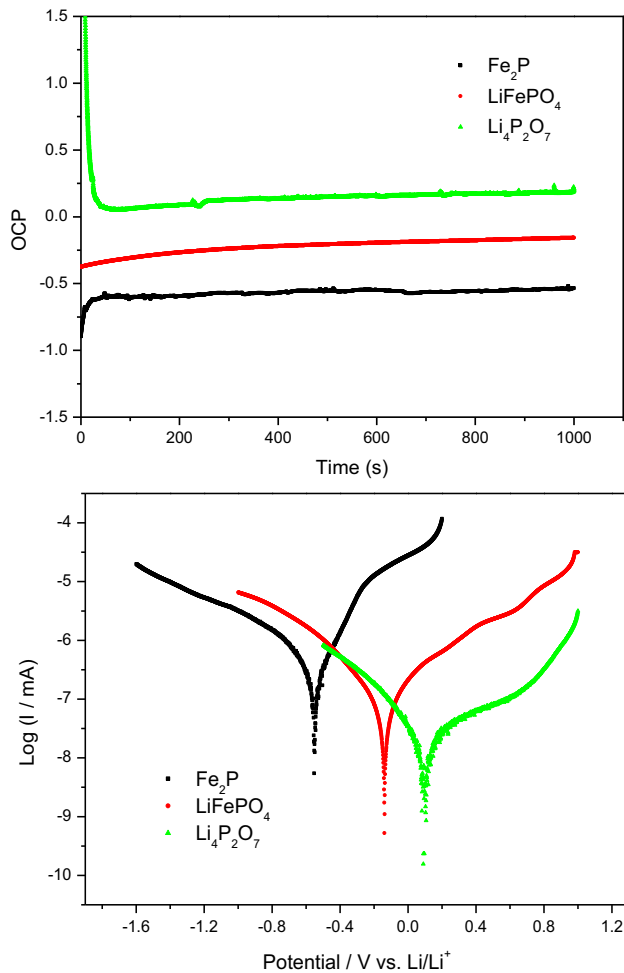
Fig. 7. Open circuit potential and Tafel plots of the samples.

influence of these impurity phases on carbon coating has been reported in our previous work [31]. Here, our focus is on the surface aging process and the relationship between impurity phase and LiFePO$_4$.

To investigate the surface aging (corrosion) process, the polished LiFePO$_4$ was stored in 1 M LiPF$_6$ solutions contaminated with 400 ppm H$_2$O at room temperature. This water-contaminated electrolyte was considered as a corrosive medium to accelerate the surface corrosion as HF often form with the following widely-accepted mechanism [32,33],

$$LiPF_6 = LiF + PF_5 \qquad (1)$$

$$PF_5 + H_2O = POF_3 + 2HF \qquad (2)$$

Fig. 4 shows SEM images of the surface corrosion process at LiFePO$_4$ ingot sample with various stored time. The polished fresh LiFePO$_4$ shows a smooth surface with some grain boundaries (bright zone) where iron-rich impurity phase generally exist (Fig. 4a), as discussed above. After 8 h storage in H$_2$O-contaminated LiFePO$_4$ (Fig. 4b), obvious corrosion phenomenon began at these iron-rich grain boundaries, and iron began to dissolve (EDX analysis). With 24 h aging process, more serious corrosion occurred at these impurity phase, as the brighter and coarser image shown in these boundaries in Fig. 4c. EDX also showed more iron loss. After 32 h aging process, the grain boundaries got deeper and deeper, some new boundaries were created along the initial boundaries on the surface (marked in green in the web version), further aggravating the corrosion process. Although the overall surface of the ingot sample was also corroded by the possible chemical reaction with HF, the more serious corrosion only occurred at the iron-rich grain boundaries while the adjacent LiFePO$_4$ bulk underwent negligible change, indicating the iron-rich impurity phase may "protect" the adjacent LiFePO$_4$ from serious corrosion. This will be explained later on.

The further chemistry of the corroded surface at iron-rich zone was characterized by TOF-SIMS analysis. Fig. 5 shows the highlighted TOF-SIMS map collected from the aged sample surface, showing the distribution of chemical species on the surface. The selected zone comes from the grain boundaries (marked in Fig. 5a) where iron element is rich. As shown in Fig. 5b, the brighter color follows the same shape in marked zone in Fig. 5a, indicating that iron element rich was indeed found at the boundary. Interestingly, much more F element was also found along the boundary due to
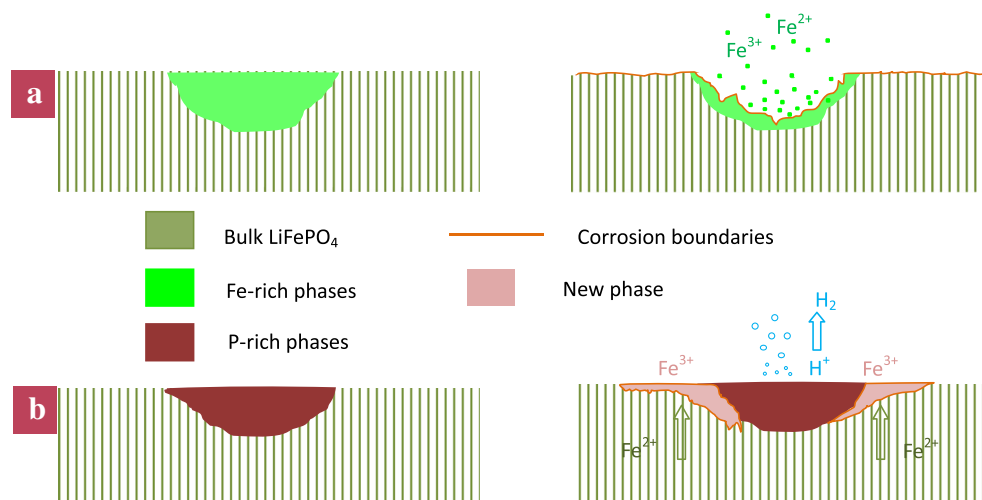
impurity phases separated from LiFePO$_4$ and located at the boundaries [25]. These impurity phases often appear during the LiFePO$_4$ synthesis by other methods especially in solid-state condition. The presence of these impurity phases definitely affects the surface chemistry and property of LiFePO$_4$, and a visualization study of the


Fig. 8. The possible corrosion mechanism at the iron-rich (a) and phosphorus–rich (b) phases on LiFePO$_4$.

the corrosion process, matching well the iron element distribution. At the same time, FeF fragment was also rich at this area. This SIMS map information further confirmed that the corrosion process is much worse at iron-rich zones, which is consistent with the above EDX results.

In addition to iron-rich phases, the effects of the other impurity phases (phosphorus-rich phases) on surface corrosion were also investigated. Compared with iron-rich phases, these phosphorus-rich phases reveal a completely different corrosion mechanism. As SEM image and EDX shown in Fig. 6, with the aging time, more and more serious corrosion behavior was observed at the bulk $LiFePO_4$ zone near to the phosphorus-rich phase's gain boundaries. Interestingly, EDX results indicate that the adjacent bulk $LiFePO_4$ shows no obvious iron loss (dissolution) although an increase of F peak was found at this phosphorus-rich impurity phases. The increase of F peak indicates a serious corrosion occurred at these zones, but, interestingly, iron was not dissolved much here. Therefore, a different corrosion mechanism from the above iron-rich phase may be presented here, which may be attributed to the different corrosion potentials among the different impurity phases due to the inhomogeneous chemistry composition.

In order to elucidate the different corrosion mechanisms and the relationships between impurity phase and $LiFePO_4$ bulk materials, an electrochemical Tafel analysis is carried out on the standard commercial samples ($LiFePO_4$, Fe_2P and $Li_4P_2O_7$ powders) (Fig. 7). The open circuit potentials (OCP) in the electrolyte where the rates of the anodic and cathodic processes are balanced for the samples were firstly recorded. Theoretically, the corrosion potential U_{corr} is equal to the OCP measured in dependence on exposure time prior to the polarization experiment. The OCPs for $Li_4P_2O_7$, $LiFePO_4$ and Fe_2P were revealed to be around 0.20 V, −0.15 V, and −0.53 V, respectively. The Tafel curves were obtained by sweeping the voltage from the OCP using a low scan rate of 0.2 mV s^{-1}. Compared with $LiFePO_4$, it is notable that the curve of $Li_4P_2O_7$ is shifted to higher potentials and significantly lower corrosion current while Fe_2P sample is quite the reverse. Remarkably, among the three commercial samples, $Li_4P_2O_7$ is the most stable in electrolytes while Fe_2P is the least.

Considering the different corrosion potentials among the above impurity phases, Fig. 8 shows the possible corrosion mechanisms of the above two types of impurity phase in $LiFePO_4$. The iron-rich impurity phases (Fig. a) were more easily attacked directly by HF arising from Eq. (1) through the following reaction,

$$Fe - rich\ impurity\ phases + HF = FeF_x + H_2O \tag{3}$$

$$and/or\quad Fe^{2+} = Fe^{3+} \tag{4}$$
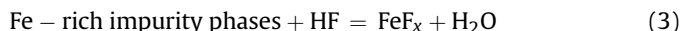
Therefore, the iron-rich impurity phase undergo serious corrosion process due to the lower corrosion potential while the adjacent shows less change, which is supported by the wide detection of F element on those two areas with EDX and SIMS techniques.

For the phosphorus-rich phases, it shows a different corrosion mechanism. The impurity phase is more stable due to higher corrosion potential compared to $LiFePO_4$; thus the aging process occurs through the following oxidation−reduction mechanism,

$$at\ P - rich\ phases,\quad H^+ + e^- = H_2 \tag{5}$$

$$at\ the\ adjacent\ bulk\ LiFePO_4\ zones,\quad Fe^{2+} = Fe^{3+} + e^- \tag{6}$$
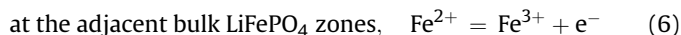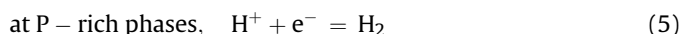
Here, the product of Fe^{3+} in olivine system could be some common chemical states such as $FePO_4$, $LiFePO_4(OH)_x$, $Li_3Fe_4(PO_4)_3$. Based on the above EDX results, lots of F signals were detected and no obvious iron was lost at this adjacent bulk $LiFePO_4$ zones. Therefore, the most possible Fe^{3+} in this study is from $LiFePO_4(OH)$

because only this alkaline product reacts with HF and produce F signal while keeps iron unchanged, with a mechanism such as

$$LiFePO_4 + H_2O = LiFePO_4(OH) + 1/2H_2 \tag{7}$$

$$Li_xFe(PO_4)(OH)_x + xHF = LiFePO_4F \tag{8}$$
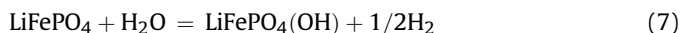
The increasing F signals and the stable iron peak in the EDX support this hypothesis.

The above study indicates that serious corrosion occurs at $LiFePO_4$ through Fe dissolution or oxidations, which are directly related to the presence of those impurity phases. These undesirable reactions will lead to irreversible changes in the $LiFePO_4$ structure and the formation of inactive phases, contributing to the capacity fade. In addition, the dissolved iron ions could be reduced to metallic clusters and deposited on negative electrodes, bringing more safety issues. In this study, we provided the comprehensive understanding of the reaction mechanisms related to the impurity phases. It should be mentioned that the practical commercial $LiFePO_4$ may not undergo such a serious corrosion due to the relatively low impurity phases amounts and especially the protection role from a surface carbon coating layer. The carbon protective role has been symmetrically studied and confirmed in our work [34].

4. Conclusions

In summary, for the first time, we provided the direct visual observation of surface corrosion process at olivine $LiFePO_4$ and the significant effects of typical impurity phases on $LiFePO_4$ corrosion. The moisture-contaminated $LiPF_6$ electrolyte was applied as the corrosion medium due to the presence of HF, which attacks $LiFePO_4$ surface and results in iron dissolution. The ingot sample with a flat surface was used as the model material to allow us to investigate the surface corrosion process in detail. Two types of impurity phase, iron-rich and phosphorus-rich phases, were identified at the surface of $LiFePO_4$ ingot. The presence of these two types of impurity phase has significant important effects on $LiFePO_4$ corrosion process. In the case of iron-rich impurity phase, the surface corrosion began from these impurity phase, and more serious iron dissolution was found, which also affects the overall surface stability. For the phosphorus-rich phases, the corrosion underwent an oxidation-reaction process, similar to an electrochemical cell in a common metal corrosion process. Therefore, the adjacent bulk $LiFePO_4$ of these phosphorus-rich impurity phases underwent an oxidation process from Fe^{2+} to Fe^{3+}. Our results provide a comprehensive understanding the fundamental corrosion process of $LiFePO_4$, and indicate that the presence of impurity phases has critical influence on the $LiFePO_4$ stability. Therefore, in addition to better control of $LiFePO_4$ purity, it is more desirable to avoid high-corrosion-potential impurity phases during synthesis and production. Moreover, applying effective surface protective layers (i.e. carbon, metal oxides) especially ultra-thin coatings deposited by advanced coating techniques such as atom layer deposition technique is essential for $LiFePO_4$ and other cathode materials in future better safe batteries [35].

References

[1] K. Padhi, K.S. Nanjundaswamy, J.B. Goodenough, J. Electrochem. Soc. 144 (1997) 1188−1194.
[2] J.B. Goodenough, Y. Kim, Chem. Mater. 22 (2010) 587−603.

[3] B.L. Ellis, K.T. Lee, L.F. Nazar, Chem. Mater. 22 (2010) 691–714.
[4] J. Wang, X. Sun, Energy Environ. Sci. 5 (2012) 5163–5185.
[5] L.X. Yuan, Z.H. Wang, W.X. Zhang, X.L. Hu, J.T. Chen, Y.H. Huang, J.B. Goodenough, Energy Environ. Sci. 4 (2011) 269–284.
[6] L. Castro, R. Dedryvère, J.-B. Ledeuil, J. Bréger, C. Tessier, D. Gonbeau, J. Electrochem. Soc. 159 (2012) A357–A363.
[7] P. Liu, J. Wang, J. Hicks-Garner, E. Sherman, S. Soukiazian, M. Verbrugge, H. Tataria, J. Musser, P. Finamore, J. Electrochem. Soc. 157 (2010) A499–A507.
[8] J. Wang, P. Liu, J. Hicks-Garner, E. Sherman, S. Soukiazian, M. Verbrugge, H. Tataria, J. Musser, P. Finamore, J. Power Sources 196 (2011) 3942–3948.
[9] M. Dubarry, B.Y. Liaw, M.S. Chen, S.S. Chyan, K.C. Han, W.T. Sie, S.H. Wu, J. Power Sources 196 (2011) 3420–3425.
[10] K. Amine, J. Liu, I. Belharouak, Electrochem. Commun. 7 (2005) 669–673.
[11] M. Koltypin, D. Aurbach, L. Nazar, B. Ellis, J. Power Sources 174 (2007) 1241–1250.
[12] M. Dubarry, B.Y. Liaw, J. Power Sources 194 (2009) 541–549.
[13] Y. Zhang, C.Y. Wang, X. Tang, J. Power Sources 196 (2011) 1513–1520.
[14] Z. Li, L. Lu, M. Ouyang, Y. Xiao, J. Power Sources 196 (2011) 9757–9766.
[15] H.F. Jin, Z. Liu, Y.M. Teng, J.K. Gao, Y. Zhao, J. Power Sources 189 (2009) 445–448.
[16] M. Cuisinier, J.-F. Martin, N. Dupre, R. Kanno, D. Guyomard, J. Mater. Chem. 21 (2011) 18575–18583.
[17] S.B. Peterson, J. Apt, J.F. Whitacre, J. Power Sources 195 (2010) 2385–2392.
[18] M. Koltypin, D. Aurbach, L. Nazar, B. Ellis, Electrochem. Solid State Lett. 10 (2007) A40–A44.
[19] S.C. Nagpure, S.S. Babu, B. Bhushan, A. Kumar, R. Mishra, W. Windl, L. Kovarik, M. Mills, Acta Mater. 59 (2011) 6917–6926.
[20] K. Zaghib, M. Dontigny, P. Charest, J.F. Labrecque, A. Guerfi, M. Kopec, A. Mauger, F. Gendron, C.M. Julien, J. Power Sources 185 (2008) 698–710.
[21] A. Ait-Salah, A. Mauger, K. Zaghib, J.B. Goodenough, N. Ravet, M. Gauthier, F. Gendron, C.M. Julien, J. Electrochem. Soc. 153 (2006) A1692–A1701.
[22] N. Ravet, M. Gauthier, K. Zaghib, J.B. Goodenough, A. Mauger, F. Gendron, C.M. Julien, Chem. Mater. 19 (2007) 2595–2602.
[23] K. Zaghib, N. Ravet, M. Gauthier, F. Gendron, A. Mauger, J.B. Goodenough, C.M. Julien, J. Power Sources 163 (2006) 560–566.
[24] A. Yamada, S.C. Chung, K. Hinokuma, J. Electrochem. Soc. 148 (2001) A224–A229.
[25] M. Gauthier, C. Michot, N. Ravet, M. Duchesneau, J. Dufour, G. Liang, J. Wontcheu, L. Gauthier, D.D. MacNeil, J. Electrochem. Soc. 157 (2010) A453–A462.
[26] D.D. McNeil, L. Devigne, C. Michot, I. Rodigues, G. Liang, M. Gauthier, J. Electrochem. Soc. 157 (2010) A463–A468.
[27] K. Zaghib, P. Charest, M. Dontigny, A. Guerfi, M. Lagacé, A. Mauger, M. Kopec, C.M. Julien, J. Power Sources 195 (2010) 8280–8288.
[28] S.P. Ong, L. Wang, B. Kang, G. Ceder, Chem. Mater. 20 (2008) 1798–1807.
[29] B. Kang, G. Ceder, Nature 458 (2009) 190–193.
[30] P.S. Herle, B. Ellis, L.F. Nazar, Nat. Mater. 3 (2004) 147–152.
[31] J. Wang, J. Yang, Y. Zhang, Y. Li, Y. Tang, M.N. Banis, X. Li, G. Liang, R. Li, X. Sun, Adv. Funct. Mater. 23 (2013) 806–814.
[32] S.F. Lux, I.T. Lucas, E. Pollak, S. Passerini, M. Winter, R. Kostecki, Electrochem. Commun. 14 (2012) 47–50.
[33] Z. Chen, Qin Yan, K. Amine, Y.-K. Sun, J. Mater. Chem. 20 (2010) 7606–7612.
[34] J. Wang, J. Yang, Y. Tang, R. Li, G. Liang, T.-K. Sham, X. Sun, J. Mater. Chem. A 1 (2013) 1579–1586.
[35] X. Meng, X.-Q. Yang, X. Sun, Adv. Mater. 24 (2012) 3589–3615.